# On Precision Kinematic Accelerations for Airborne Gravimetry

## Research article

Ch. Jekeli1\*,

## 1 Division of Geodetic Science School of Earth Sciences Ohio State University

#### Abstract:

Advances in accelerometer technology promise many orders of magnitude improvement in sensitivity; which, consequently, also suggest progress in Earth Science applications, such as through new airborne gravimetric systems. However, a new capability for one sensor then usually demands commensurate requirements from auxiliary sensors in order to realize its full potential. Specifically, airborne gravimetry would benefit from improved inertial accelerometry only if the kinematic acceleration derived from vehicle tracking or positioning is equally precise. The latter is investigated in this study to determine the limits in precision due to errors in modeling the numerical derivative and due to errors in the positions, themselves. Simulations with actual aircraft trajectories show that the kinematic acceleration using current positioning capability (that is, GPS or similar satellite navigation systems) can be determined to an accuracy at the sub-milligal level only with sufficient smoothing over intervals of 60 s or longer. The effects of position error still dominate over the model error, and both are many orders of magnitude greater than the predicted precision of state-of-the-art accelerometry. This suggests that airborne gravity field determination likely will profit more if the advances in inertial sensor technology are directed toward gravity gradiometry.

## Keywords:

airborne gravimetry • kinematic acceleration • numerical differentiation • central differences © Versita sp. z o.o.

Received 24-08-2011; accepted 25-09-2011

## 1. Introduction

Airborne gravimetry over the last four decades has rapidly become an operational tool for measuring the Earth's gravity field over larger regions with excellent accuracy and resolution. The entire Arctic Ocean was mapped in 1998-2002 at a resolution of better than 10 km with an accuracy of a few mGal under sponsorship from the National Geospatial-Intelligence Agency (Kenyon 2000), the Naval Research Laboratory, and the Danish National Space Center, following an extensive aerial gravity survey of Greenland (Forsberg and Brozena 1992; see also Forsberg et al. 2001). More recently, various Asian countries were mapped similarly for geodetic purposes (Mongolia, Malaysia, Taiwan, South Korea), among others, mostly by the Danish group (Forsberg and Olesen 2009).

For commercial applications, primarily oil and gas exploration, airborne gravimetry dates back to the 1980's, as a means to cover large tracts of land to seek out particular gravitational anomalies that suggest geologic traps where such deposits can accumulate (Hammer 1980, Gumert 1998). The importance of gravimetry for geophysics was also recognized and emphasized in a number of National Research Council and NASA studies of the 1990s (e.g., NASA 1991; National Research Council 1995; Dickey et al. 1997).

Advanced accelerometry based on micro-machined, solid-state devices (such as the Zero Force Accelerometer (ZFA), Draper Laboratory 2010) today portends unprecedented precision; for example, as low as 10-20 pg/ $\sqrt{\text{Hz}}$  for airborne applications and 0.5 pg/ $\sqrt{\text{Hz}}$  for the dynamically quieter environment of a satellite platform (1 pg =1 pico - g  $\approx 10^{-11}$  m/s²). Such sensitivity far exceeds that of current airborne gravimetry (where typical sensitivity is at the mgal level; 1 mgal =  $10^{-5}$  m/s²), and the question naturally arises whether it offers corresponding advantages for future



<sup>\*</sup>E-mail: jekeli.1@osu.edu

systems.

In view of the importance of airborne gravimetry and the technological developments in accelerometry, this paper attempts to answer this question. Specifically, the complementary kinematic acceleration determination from precise positions is investigated, since it is a key component in airborne gravimetry. Significant investigations in this direction exist in the literature; for example Van Dierendonck et al. (1994), Jekeli and Garcia (1997), Bruton et al. (1999), Kennedy et al. (2001), Kreye and Hein (2003), among others. Two types of error enter the computed kinematic acceleration: 1) errors in positioning, usually obtained from GPS and thus due to receiver noise, unknown tropospheric and ionospheric delays, multipath, orbital errors, etc.; and, 2) model errors associated with the numerical differentiation of discrete position coordinates. The present focus is on the latter although position error is not neglected. Indeed, the purpose is to determine the limits achievable in reducing the model error for realistic airborne trajectories, and comparing this to acceleration uncertainty induced by present-day position error, as well as to the new technology in accelerometry.

## 2. Mathematical Background

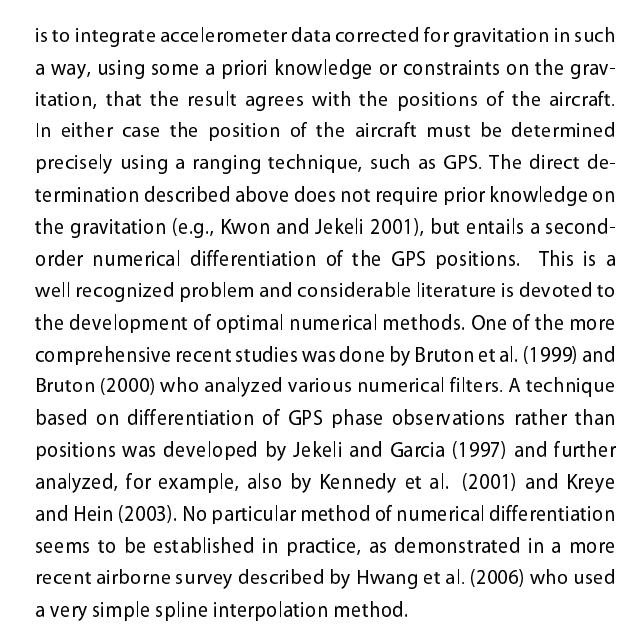
Airborne gravimetry (or, any moving-base gravimetry) is founded on Newton's Second Law of Motion in a gravitational field:

$$\ddot{x} = a + q,\tag{1}$$

where a is the inertial acceleration of the vehicle (due to action forces such as lift, drag, and propulsion), g is the gravitational acceleration due to the ambient gravitational field, and  $\ddot{x}$  is the total, kinematic acceleration of the vehicle, being the second time derivative of its position, x. Equation (1) holds in an inertial (that is, freely-falling, non-rotating) frame and assumes that inertial mass is equivalent to gravitational mass (Einstein's equivalence principle). The inertial acceleration, a, is sensed by an accelerometer; and, in order to determine  $q_i$ , the kinematic acceleration must be calculated from a numerical differentiation of observed positions. Position can be observed, or determined, using ranging methods, such as GPS. In a rotating frame, such as the one attached to the vehicle, Newton's equation of motion takes on a few extra terms (Jekeli 2000), which means that also the orientation of the platform in inertial space must be determined. But, the essential principle is the same: gravimetry requires both accelerometry and a numerical differentiation of positions obtained independently by a ranging system.

## 2.1. The Kinematic Acceleration Filter

The present focus with respect to airborne gravimetry is the determination of the kinematic acceleration,  $\ddot{x}$ . It is a necessary component of a proven method to compute the gravitational acceleration from accelerometry. The alternative, indirect approach



While all these methods can be and have been tested using data from a stationary antenna (where the true acceleration is known), the accuracy of aircraft accelerations derived from actual airborne data is more difficult to ascertain. Usually, multiple GPS tracking stations (or tracking systems) are used to compare accelerations derived from the different corresponding solutions for the aircraft trajectory. For example, Van Dierendonck et al. (1994) used two tracking stations and a laser altimeter (over a lake) to study the effects of various GPS errors on the acceleration determination. Also, Salazar et al. (2011) compared velocities and accelerations using solutions of aircraft trajectories from different tracking stations. However, as will be argued later, such comparisons primarily indicate the effect of position error. They say little or nothing about the model error (the error in the numerical differentiation), which can be large and dominate the effect of position error. For example, the comparison by Kreye and Hein (2003) of two differentiation methods using the same airborne data set yielded differences of the order of 10 mgal, significantly larger than the differences of a few mgal found by comparing accelerations derived from two equivalent data sets using the same method.

It is well known that numerical differentiation is an unstable process and model errors depend on values of the derivative two orders higher (that is, on the fourth-order derivative in case of double differentiation; e.g., Conte and de Boor 1965). This has two consequences in the analysis. First, it is difficult to simulate a truth model against which to compare different numerical differentiation methods. Second, a significant amount of smoothing (low-pass filtering) is required to obtain high accuracy in the numerical differentiation. With current tracking systems, such smoothing is also needed to reduce the effect of noise in positions. For the present analysis, suppose we have a long sequence of

position values,  $x_n$ , uniformly sampled from a continuous trajectory, x (t), with sampling interval,  $\Delta t$ . We are not concerned with

$$x(t) = \int_{-\infty}^{\infty} F_x(f) e^{i2\pi f t} df, \qquad (2)$$

where f is (cyclical) temporal frequency, then the Fourier transform of the second derivative is

$$F_{\ddot{x}}(f) = D(f) F_{x}(f), \qquad (3)$$

where

$$D(f) = -(2\pi f)^2. (4)$$

Equation (3), representing a product in the frequency domain, shows that differentiation may be viewed, according to the well known convolution theorem (Bracewell 1965), as a filter whose frequency response is given by equation (4).

One could estimate the second derivative of positions via the frequency domain: multiply the Fourier transform of the positions by  $D\left(f\right)$  and compute the inverse transform. However, the discreteness of the positions introduces considerable aliasing and the finite extent of the position data further introduces spectral leakage (ringing, or the Gibbs phenomenon). For these reasons, one typically designs a filter to mitigate these effects. We start with a finite, discrete filter (finite-length impulse response, FIR, filter) of the form

$$\ddot{x}_n = \Delta t \sum_{j=-J}^{J} d_j x_{n-j},\tag{5}$$

where J is called the order of the filter, and the filter coefficients,  $d_j$ , represent the impulse response of the filter. Since the number of coefficients is finite, the frequency response cannot equal the ideal response, D(f), equation (4). However, the coefficients should be symmetric with respect to the origin, i.e.,  $d_{-j}=d_j$ , since the ideal frequency response is real. This requires that the number of coefficients is odd, (2J+1).

To illustrate the limitations of simply applying Fourier transforms to the data, consider the filter coefficients determined from the ideal frequency response. Using the (Shannon) sampling theorem (Marple 1987) that guarantees the reconstruction of the continuous trajectory from its samples if the continuous form contains no spectral components with (absolute) frequency greater than  $f_N=1/(2\Delta t)$ , that is, the Nyquist frequency, we have

$$x(t) = \sum_{j=-\infty}^{\infty} x_j \operatorname{sinc}\left(\frac{t}{\Delta t} - j\right), \tag{6}$$

where sinc is the cardinal sine function:  $\mathrm{sinc}\left(t\right)=\mathrm{sin}\left(\pi t\right)\big/\left(\pi t\right)$ . This function is differentiable,

$$\frac{d^2}{du^2} \operatorname{sinc}(u) = \frac{2}{u^2} \left( \operatorname{sinc}(u) - \cos(\pi u) \right) - \pi^2 \operatorname{sinc}(u) , \quad (7)$$

and

## Journal of Geodetic Science

$$\frac{d^2}{du^2}\operatorname{sinc}(u)\Big|_{u=0} = -\frac{\pi^2}{3};$$

$$\frac{d^2}{du^2}\operatorname{sinc}(u)\Big|_{u=\pm j} = -\frac{2(-1)^j}{j^2}, \quad j=1,2,\dots$$
(8)

369

We thus differentiate:

$$\ddot{x}(t_n) = \sum_{j=-\infty}^{\infty} x_j \frac{d^2}{dt^2} \operatorname{sinc}\left(\frac{t}{\Delta t} - j\right)\Big|_{t=t_n}$$

$$= \frac{1}{\Delta t^2} \sum_{j=-\infty}^{\infty} x_{n-j} \frac{d^2}{du^2} \operatorname{sinc}(u)\Big|_{u=-j}, u = \frac{t}{\Delta t}$$

$$= -\frac{\pi^2}{3\Delta t^2} x_n - \frac{2}{\Delta t^2} \sum_{\substack{j=-\infty \ j\neq 0}}^{\infty} x_{n-j} \frac{(-1)^j}{j^2}$$
(9)

These second-derivative values are approximated with an FIR filter of the form of equation (5) by limiting the range of the index, *j*, since we have only a finite number of position data. We obtain:

$$d_0 = -\frac{\pi^2}{3\Delta t^3}; \quad d_{\pm j} = -\frac{2}{\Delta t} \frac{(-1)^j}{(j\Delta t)^2}, \quad j = 1, 2, \dots, J.$$
 (10)

However, by limiting the index, we also introduce a bias. That is, the filter coefficients should sum to zero to be consistent with the derivative of a constant. Hence, the coefficients need to be modified:

$$d_0 = -\frac{\pi^2}{3\Delta t^3} - s_0; \quad d_{\pm j} = -\frac{2}{\Delta t} \frac{(-1)^j}{(j\Delta t)^2} - s_0, \quad j = 1, 2, \dots, J,$$
(11)

where

$$s_0 = -\frac{\pi^2}{3\Delta t^3} - \frac{2}{(2J+1)\Delta t} \sum_{j=-J}^{J} \frac{(-1)^j}{(j\Delta t)^2}.$$
 (12)

Similarly, the second derivative of a linear trend should vanish. This is automatically satisfied for the FIR if the coefficients are symmetric ( $d_{-j}=d_j$ ), which was already noted as a requirement, and is easily shown to be the case above.

Given the filter coefficients,  $d_j$ , the frequency response can be computed from the discrete Fourier transform:

$$\hat{D}(f) = \Delta t \sum_{j=-J}^{J} d_j e^{-i2\pi\Delta t j f}.$$
 (13)

Figure 1 compares the frequency response, equation (13), to the ideal one, equation (4), for J=13 and  $\Delta t=1$  s; and, the absolute differences between them (the errors) for various orders, J, are shown in Figure 1. The oscillatory nature of the error is due to the truncation of the filter at  $j=\pm J$ . This effect (Gibb's phenomenon) can be mitigated by applying a window function to the impulse response. Bruton (2000) showed that the oscillation thus may be reduced by about an order of magnitude in the low-to mid-frequencies.

Another second-derivative filter design is a member of a class of numerical differentiators known as *central differences*. These are derived from a Taylor expansion of the function, where from (Khan and Ohba 1999) we have the following general formula (modified

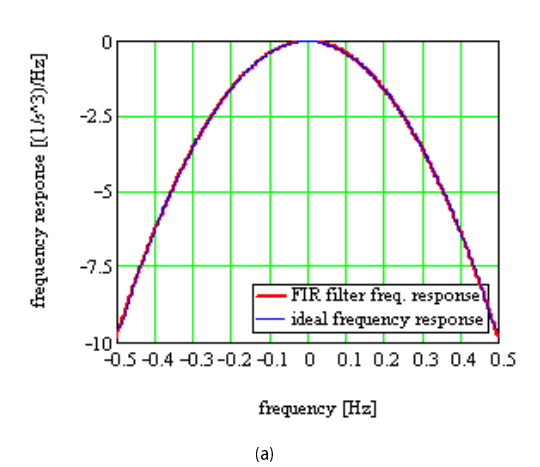


Figure 1. a) Frequency response of the approximation to the ideal second-derivative FIR filter, *J* = 13; b) the error for various indicated orders.

slightly) for the second derivative using 2J + 1 evenly spaced points,

$$\ddot{x}_n = \Delta t \sum_{j=-J}^{J} d_{J,j} x_{n-j}, \tag{14}$$

with

$$d_{J,0} = -2\sum_{i=1}^{J} d_{J,j},\tag{15}$$

and for  $j = \pm 1, \ldots \pm J$ ,

$$d_{J,j} = (-1)^{j+1} \frac{2}{\Delta t (i\Delta t)^2} \frac{(J!)^2}{(J-j)! (J+j)!}.$$
 (16)

For J=1, we get  $d_{1,\pm 1}=1/\Delta t^3$  and  $d_{1,0}=-2/\Delta t^3$ , leading to the well-known double difference formula:

$$\ddot{x}_n = \frac{1}{\Delta t^2} \left( x_{n-1} - 2x_n + x_{n+1} \right). \tag{17}$$

VERSITA

A recursion formula for the filter coefficients,  $d_{I,i}$ , is easily found:

$$d_{J,j} = -\left(1 - \frac{1}{j}\right)^2 \frac{(J-j+1)}{(J+j)} d_{J,j-1},$$
  

$$d_{J,-j} = d_{J,j}, \quad j = 2, \dots, J; \quad d_{J,1} = \frac{2J}{(J+1)\Delta t^3}.$$
(18)

It is noted that the filter coefficients sum to zero in view of equation (15).

The frequency response of this filter is given by substituting equations (15) and (16) into equation (13). The responses for a sampling interval of  $\Delta t=1$  s and different values of J are illustrated in Figure 2; and errors relative to the ideal response are shown in Figure 2. Clearly, the approximation improves as J increases. Compared to the previous approximation of the ideal response, equations (11), the central difference filter is much more accurate at low frequencies, but worse at high frequencies (e.g., compare Figures 1 and 2 for  $|f| \geq 0.4$  Hz when J=13).

Bruton (2000) also mentions the use of the Parks-McClellan algorithm that is based on the Remez exchange algorithm (Parks and McClellan 1972) to design an optimal (minimax) FIR filter that is most efficient (fewest number of filter coefficients) in meeting specified accuracy requirements over a particular spectral band. His example shows, compared to the simple filter, equation (11), that the error thus can be reduced by several orders of magnitude over the entire spectral band of interest. However, at the lower frequencies in which we are ultimately interested, the central-difference filter is still more accurate, as seen in Figure 2. It is also noted that the Parks-McClellan/Remez method is an iterative process that may not always converge and may have other instabilities. The central difference method is very stable and is the method of differentiation often used for GPS kinematic accelerations (e.g., Kennedy et al., 2001, Salazar et al. 2011).

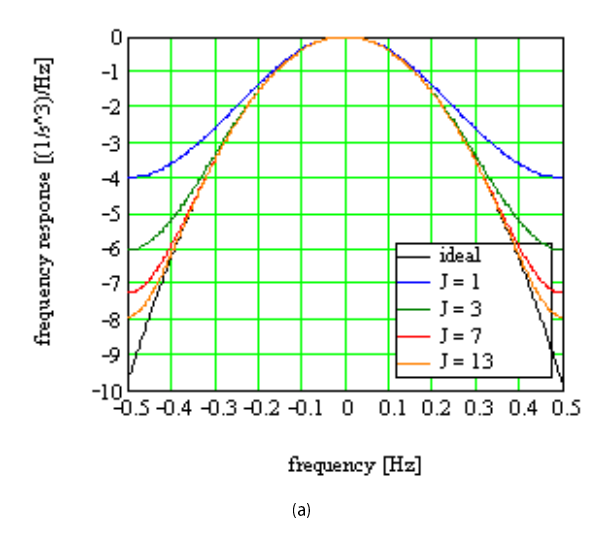
## 2.2. A Mutually Consistent Model

Evaluating the performance of the central-difference differentiation filter in practical applications requires a reasonably realistic truth model. For a given realism (e.g., the dynamics of an aircraft trajectory), the difficulty is to devise a truth model that yields mutually consistent positions, x, and accelerations, a+g (or, even just a), according to equation (1).

One approach, for the model,  $\ddot{x} = a$ , is to integrate accelerations from a starting time,  $t_k$ , to get positions at some later time, t:

$$x(t) = x(t_k) + \dot{x}(t_k)(t - t_k) + \int_{t_k}^{t} (t - t') a(t') dt', (19)$$

(which can be checked by differentiating twice). The velocity at  $t_k$  can be eliminated if also the position at  $t_{k+1}$  is known. If the interval between epochs of the desired positions is constant  $(t_{k+1}-t_k=\Delta t,$  for all k), then we find that the positions are determined recursively according to



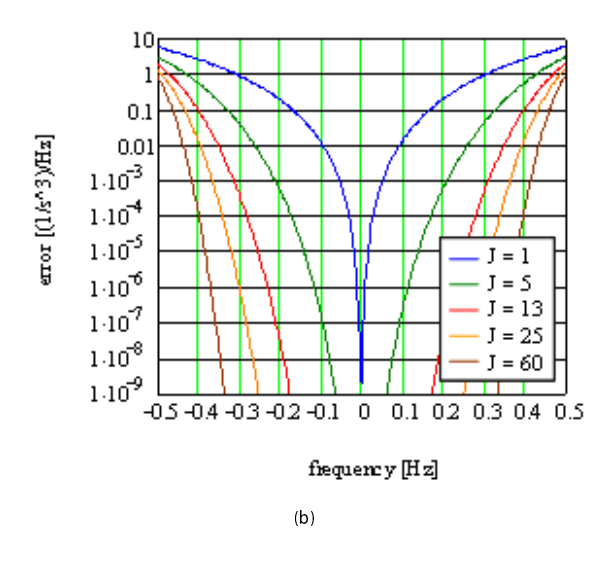


Figure 2. a) Frequency response of central difference filters for the second derivative and for various orders; b) errors of these frequency responses relative to the ideal response.

$$x_{k+2} = -x_k + 2x_{k+1} + \int_{t_k}^{t_{k+1}} (t' - t_k) a(t') dt' + \int_{t_{k+1}}^{t_{k+2}} (t_{k+2} - t') a(t') dt'.$$
 (20)

Performing the integration requires some truth model for the accelerations. We may choose actual measured airborne accelerometer data, but taken as errorless, and any suitable interpolating function for which the integrals can be evaluated. For a given set of accelerometer data, each choice of interpolating function yields a different "true" position sequence that is consistent with the accelerometer data.

The alternative is to start with position data, obtained from GPS, and assumed errorless. These are interpolated with an appropriate analytic function that is then differentiated to yield mutually

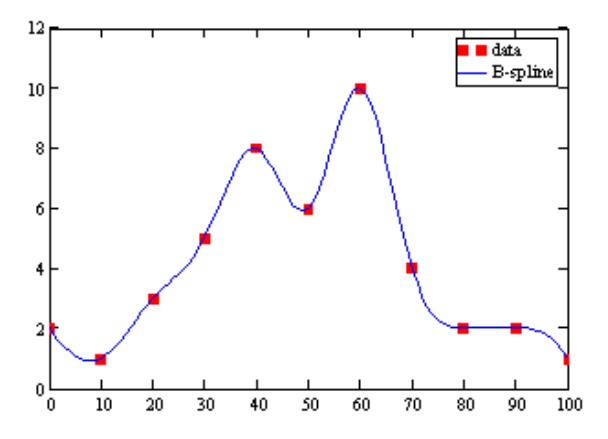


Figure 3. Example of position data interpolated by B-splines.

consistent accelerations. But, this begs the question of analyzing the numerical differentiation filter. In a sense, however, we face the same dilemma as above. A numerical approximation is needed to create a mutually and perfectly consistent set of position and acceleration data; and yet, we wish to test the numerical approximation to go from one to the other. Both approaches described above (from accelerations to positions, or vice versa) are essentially identical; neither solves the dilemma and both create the same problem.

The only solution is to compare two numerical differentiation operators, where one is treated as correct in the sense of creating a mutually consistent position/acceleration data set. This is similar to a perturbation method, where the perturbation in the model may or may not be a realistic quantification of the error. On the other hand, for the perturbation used here, one may argue that it fails on the optimistic side of assessing the errors. With these caveats, the second approach above is pursued by comparing the centraldifference accelerations to accelerations obtained by interpolating a given set of positions using fifth-order B-splines (Schumaker 1993; see Figure 3 for an illustration). These B-splines are piecewise polynomials differentiable everywhere up to third order, so that the second derivatives at the data points are smooth. Although they are based on local support, the derived accelerations have very little high-frequency content beyond the Nyquist frequency (shown later). Both being derived from polynomials, the numerical results of comparing central-difference and B-spline accelerations will be optimistic. On the other hand, they provide reasonable answers to our performance questions as functions of various salient parameters.

## 3. Numerical Tests

With a view toward the airborne gravimetry application, GPS data from an airborne survey were used to simulate the dynamics of the trajectory. The data comprise precise GPS solutions, based



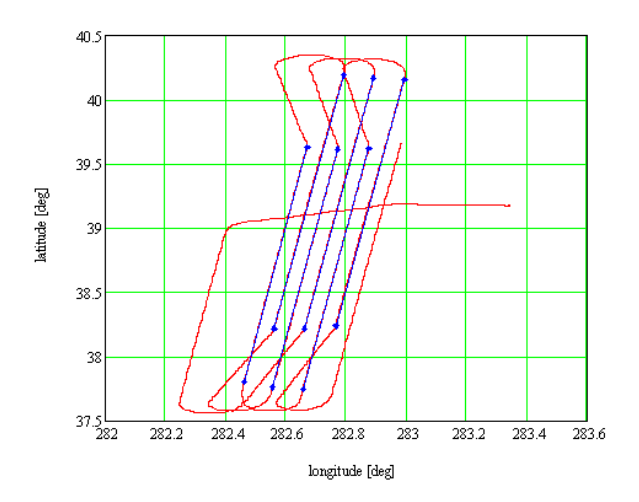


Figure 4. Airborne gravimetry trajectory of Flight 0211 conducted by Intermap Technologies Corp. in 1999 over the Baltimore/Washington, D.C. area. Blue segments (numbered 1 through 6, from left to right) indicate the parts of the trajectory that were analyzed for the kinematic acceleration determination.

on 2 Hz data from Ashtech receivers, of an aircraft trajectory that was one of several flown over the Baltimore/Washington, DC, area in 1999 by Intermap Technologies Corp. for the purpose of measuring the gravity field. It is shown in Figure 4 together with the segments along which the true accelerations were simulated. Here and later, using another airborne GPS trajectory, it is assumed that the estimated positions are free of the effects of cycle slips and other systematic errors. The determined positions (Cartesian coordinates), thus assumed true, were interpolated by fifth-order B-splines. This piecewise polynomial was then differentiated twice to obtain "true" accelerations at the 2 Hz data points. The errors in the accelerations are the differences between the central differences of order, J, and the B-spline accelerations for each of the segments and in each of the coordinates. The corresponding standard deviations, per segment and coordinate, were computed according to

$$\sigma_{\delta \ddot{x}} = \sqrt{\frac{1}{N} \sum_{k=0}^{N-1} \left( \delta \ddot{x}_k - \frac{1}{N} \sum_{k=0}^{N-1} \delta \ddot{x}_k \right)^2},$$
 (21)

where N is the total number of points in the segment, and  $\delta\ddot{x}_k$  is the  $k^{th}$  error in the segment. Figure 5 shows the standard deviations of the errors. The errors (i.e., differences) stabilize with increasing order at a level of about 200-500 mgal. Orders higher than about J=120 offer no substantial decrease in error. In all cases the mean error, the second term in the bracket in equation (21), was not significantly different from zero at the sub-mgal level.

The sensitivity of the acceleration error to the dynamics of the trajectory is illustrated in Figure 6. Here, the standard deviation of the acceleration error for J=240 is plotted against the standard

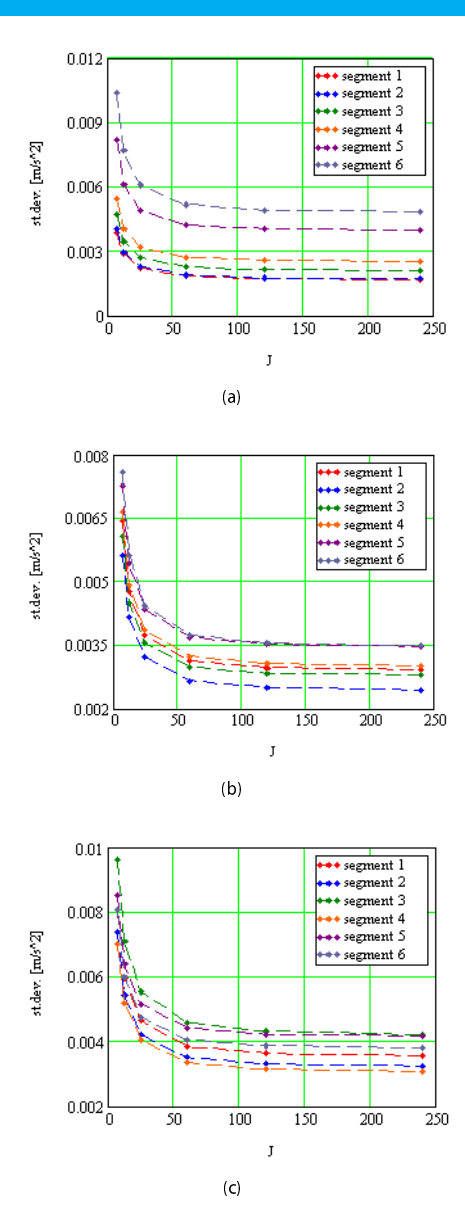


Figure 5. Standard deviations of errors in acceleration as function of central-difference order for each of the coordinates, *x* (top), *y* (middle), *z* (bottom), and for each of the segments in Figure 4.

deviation of the acceleration, itself, for each segment and each coordinate. The error is almost directly proportional to the level of dynamics of the moving platform. The variation in dynamics observed for this trajectory from segment to segment may be due to actual changes in turbulence, or it may be due to changes in error behavior in the position solution.

The limiting accuracy of several hundred mgal agrees with test results recently reported by Salazar et al. (2011) who used a central-difference filter with J=5. For differential GPS solutions between



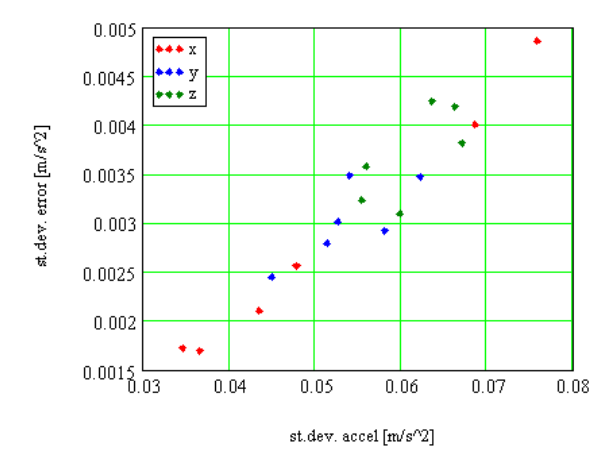


Figure 6. Sensitivity of the error in the numerically determined acceleration to the dynamics environment of the moving platform. Each data point represents a coordinate and a segment.

base stations 142 km apart (where the true acceleration is zero), they found standard deviations in the computed acceleration of the order of several mm/s<sup>2</sup>. We surmise that the use of an actual dynamic trajectory is responsible for the need to use higher order filters

One may wish to consider a higher sampling rate in order to capture the high—frequency details of the accelerations with the aim to reduce the error in the numerically determined acceleration. The analysis here is limited to an artificial simulated trajectory at these higher frequencies, since no high frequency airborne GPS data were available. The sampling rate is increased to 20 Hz, but even higher rates could be considered (GPS receivers now yield up to 100 Hz data rates). One option is simply to use the B-spline interpolation already computed from the given trajectory (2 Hz, in this case) and sample it at higher resolution. However, we see in Figure 7 that the higher-frequency acceleration thus simulated is not realistic, when compared to the accelerations of the Intermap trajectories that were sensed by the on-board accelerometers.

Instead, we add high-frequency content to the existing trajectory according to an algorithm that results as far as possible in a realistic acceleration power spectral density (psd). Experiments have shown that simply introducing a random, zero-mean, spectral component scaled by the acceleration power spectrum creates too much dynamics. Instead, we consider the method of simply adjusting the existing phase and amplitude spectra (from the B-spline-interpolated, high-resolution model) at each higher frequency in some random manner. To simplify the analysis (and since the accelerations for all three coordinates behave similarly), we consider only a single coordinate — the height above a reference surface, such as the Earth ellipsoid.

If  $H_k = c_k + id_k$  is the spectral component of a B-spline inter-

polated height coordinate for wave number, k, then in terms of amplitude and phase, we have

$$H_k = \sqrt{c_k^2 + d_k^2} e^{i \tan^{-1}(d_k/c_k)} = b_k e^{i\psi_k}.$$
 (22)

We alter the amplitude and phase as follows:

$$\hat{b}_k = b_k (1 + v_k) \,, \tag{23}$$

$$\hat{\psi}_k = \psi_k \left( 1 + w_k \right), \tag{24}$$

where  $v_k \sim N\left(0,\sigma_v^2\right)$ ,  $w_k \sim N\left(0,\sigma_w^2\right)$  are normally distributed random variables with adjustable variances to ensure that the dynamics of the resulting trajectory is reasonable. For  $\sigma_v^2 \rightarrow 0$  and  $\sigma_w^2 \rightarrow 0$ , the original B-spline trajectory would be obtained.

The alternate spectrum is then  $\hat{H}_k = \hat{b}_k e^{i\hat{\psi}_k}$  and the heights according to this model are given continuously by utilizing a new B-spline interpolation, as before. In order to obtain a real representation of the heights (as opposed to a set of complex numbers), the frequency and time domains must be shifted appropriately. Also, we assume that the number of time domain points, N, is odd. Thus, if  $t_0 \leq t \leq t_1$ , then with  $N\Delta t = t_1 - t_0$ , and

$$\hat{H}_k = \Delta t \sum_{\ell=0}^{N-1} h\left(t_0 + \ell \Delta t\right) e^{-i\frac{2\pi}{N}k\ell},\tag{25}$$

one has

$$h(t) = \frac{1}{N\Delta t} \sum_{k=-\frac{N-1}{2}}^{\frac{N-1}{2}} \hat{H}_k e^{i\frac{2\pi}{N\Delta t}k(t-t_0)},$$
 (26)

where it is noted that  $\hat{H}_{N-k} = \hat{H}_k^*$  and  $\hat{H}_{N+k} = \hat{H}_k$ .

Figure 7 shows the acceleration psd for the 20-Hz B-spline trajectory (interpolated from the original 2 Hz data and computed using the corresponding analytic accelerations); the psd of the actual 25-Hz vertical accelerations sensed by Intermap accelerometers; and, the acceleration psd of the 20-Hz trajectory altered by replacing spectral components beyond 1 Hz with components scaled according to equations (23) and (24) by random Gaussian variables having standard deviation,  $\sigma_v = \sigma_w = 0.0002$ . The altered-trajectory accelerations were again determined from a 5<sup>th</sup>-order B-spline interpolation. We see that the accelerations of the original B-spline interpolated trajectory have virtually no power beyond the Nyquist frequency, 1 Hz, of the given 2-Hz trajectory. The acceleration psd of this trajectory, however, contains a significant resonance just below 1 Hz, compared to the actual acceleration psd from accelerometers. This may be due to aliasing error in the spectrum of the given 2-Hz trajectory. The upward trend of the psd of the altered trajectory for frequencies greater than about 1.2 Hz is due to the random nature of the alteration (white noise in position is amplified by the square of frequency for accelerations). Increasing  $\sigma_v$  and  $\sigma_w$  moves this ramp up in amplitude. The modified-trajectory accelerations have no power beyond 10 Hz, which is its Nyquist limit.



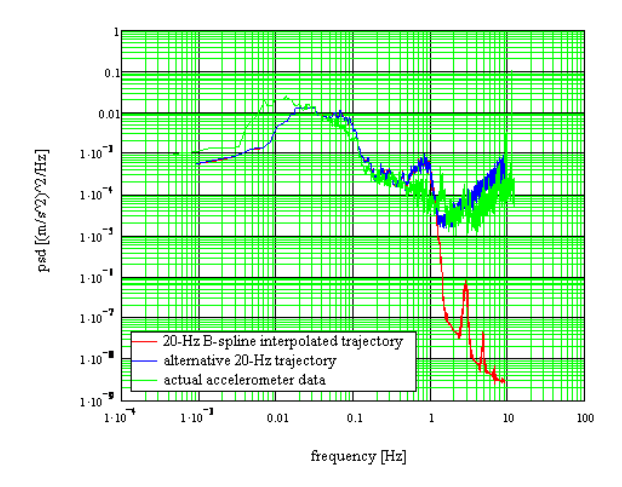


Figure 7. PSD's of accelerations determined directly from the Fourier transforms of the indicated signals, and median-smoothed over a 31-frequency window.

Using this modified trajectory in heights, the central-difference differentiator was applied with varying order, J. The 20 Hz trajectory was also decimated to 10 Hz, 5 Hz, and 2 Hz to simulate lower resolution data. Figure 8 shows the standard deviations of the differences between the numerically determined acceleration and the "true" accelerations based on the B-spline interpolation of the 20 Hz data. We see that when there is significant high frequency content in the data beyond the Nyquist limit (the 2 Hz, 5 Hz, 10 Hz trajectories), then the error is almost independent of the order of the numerical differentiation operator. And, when there is practically no spectral content beyond the Nyquist frequency (20 Hz trajectory), the accuracy improves dramatically with increasing J, but not better than for the original 2 Hz simulated trajectory (where the standard deviation for J = 25 ranged between 0.0032 m/s<sup>2</sup> and  $0.0046 \text{ m/s}^2$ , for the three coordinates, versus  $0.0078 \text{ m/s}^2$ for the 20-Hz trajectory). Thus, a higher sampling rate does not reduce the numerical differentiation error if there exists significant dynamics at these higher frequencies (as would be the case in an aircraft environment).

The only method to bring about a substantial reduction in model error is smoothing. The original 20-Hz "true" accelerations, from modified positions as described above, were smoothed using a simple (unweighted) moving average over various time windows. Then they were decimated for the comparison to the accelerations determined by numerical differentiation of the decimated data followed by the same smoothing (Figure 9). The decimated data all yield roughly equal results, all worse than the results for the 20-Hz data, likely because there remains some spectral content beyond the Nyquist limit due to the imperfect frequency response of the smoother. However, the errors now are in the range of a few mgal, which is required for airborne gravimetry.

Figure 10 shows psd's of the accelerations derived from the simu-



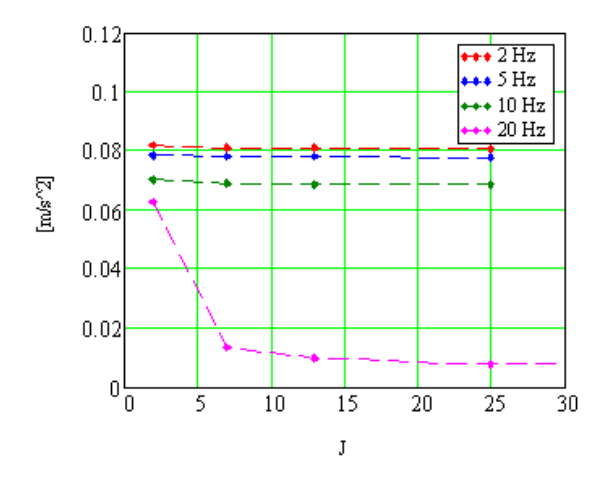


Figure 8. Standard deviations of the numerical acceleration errors for different resolutions of the 20-Hz height trajectory, as a function of the order of the central-difference numerical differentiation operator.

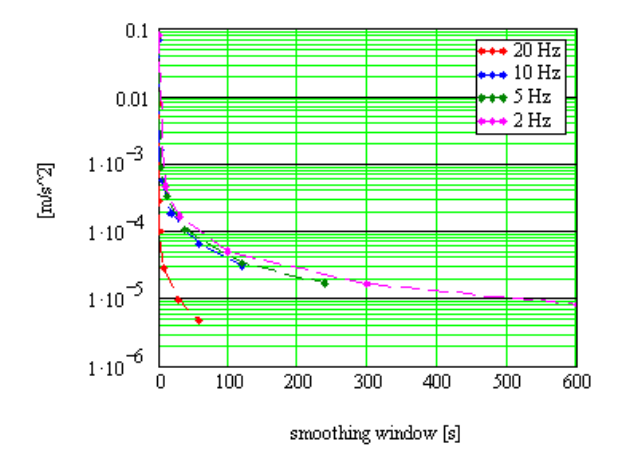


Figure 9. Standard deviations of the errors in numerical acceleration errors for different smoothing windows and data resolutions.

lated data. We see that the decimated unsmoothed accelerations have much more power than the original 20-Hz accelerations. This is caused by aliasing, which occurs across the entire spectrum because of the significant power at the very high frequencies, for example, from 5 Hz to 10 Hz, in the original 20-Hz signal. Thus, the acceleration errors for the decimated data are significantly larger than for the 20-Hz data (which explains the results of Figure 8). On the other hand, the decimated smoothed accelerations are affected by aliasing mostly at the high frequencies, where some residual power exists beyond the Nyquist frequency (5 Hz, in the illustrated case), but not of the same magnitude as the signal at lowerfrequencies. Thus, the errors for the decimated data in Figure

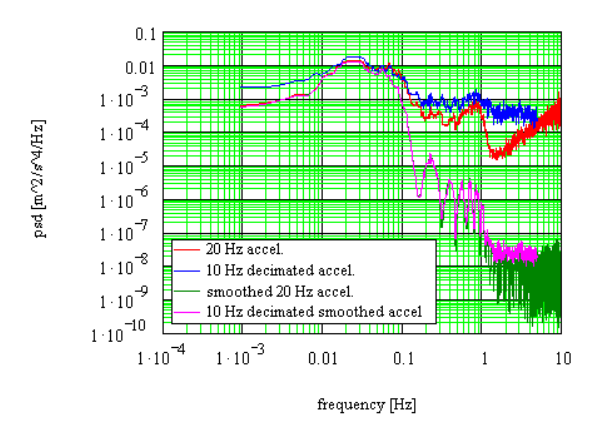


Figure 10. PSDs of 20 Hz accelerations (red) and their smoothed values over a 2.15 s window (green). Also, shown are the psd's of the 10 Hz decimations of the 20 Hz data (blue) and the smoothed 20 Hz data (magenta). All psd's were median-smoothed over 31 values.

9 are still larger than for the 20-Hz data, but also are relatively small because of the smoothing.

Finally, we consider the effect of position error on the calculation of acceleration. In order to obtain a realistic quantification of the position error of an airborne trajectory geolocated with GPS, a particular aircraft trajectory was employed whose position accuracy can be determined. This trajectory (designated "141y") was flown to map the topography over a section of the San Andreas Fault using Lidar (Shan et al. 2007) where several GPS base stations were established to test the precision of the differential GPS data processing. The map view of the trajectory is shown in Figure 11 (starting in the upper left corner), together with the profile of heights (above the WGS84 ellipsoid), as well as the locations of 12 GPS base stations. Not all 12 corresponding solutions span the same time interval, and some solutions have data gaps. The trajectory shown in Figure 11 is common, over a span of 2.65 hours, to 5 solutions that also have no gaps. It has greater dynamics than typical airborne gravimetry trajectories (as in Figure 4), but that should not affect the positioning accuracy significantly.

The multiple solutions for the aircraft trajectory offer a reasonable indication of the position errors. The residual of an individual solution with respect to the mean of the 5 solutions chosen to represent the true simulated trajectory is interpreted as the (negative) error. The power spectral densities for two such residuals over the length of the trajectory (for all three Cartesian coordinates) are shown in Figure 12. Clearly, the residuals have correlated components in the low-to-mid frequencies, and only bottom out as white noise at frequencies higher than 0.2 Hz.

The standard deviations of the residuals for all coordinates vary between 0.6 cm and 1.7 cm. The accuracy in position (using the GPS carrier signals) depends on various factors, ranging from un-modeled signal propagation delays to multipath effects and

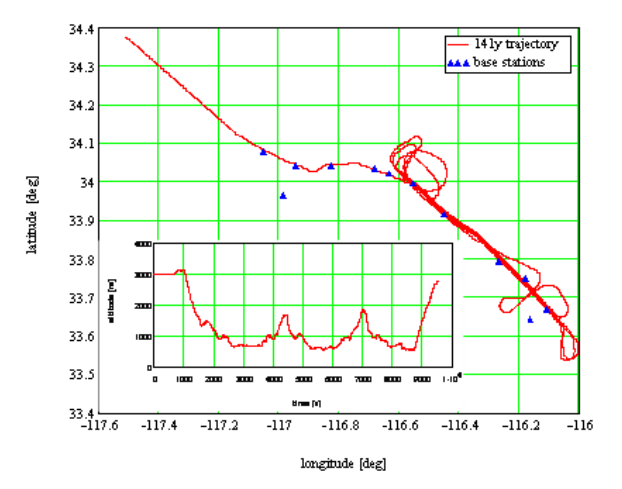
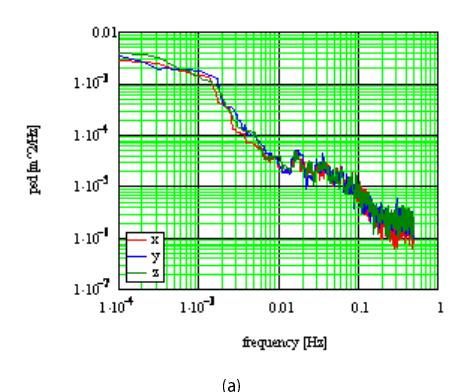


Figure 11. Trajectory of flight 141y, including base station locations used to process the GPS solutions.



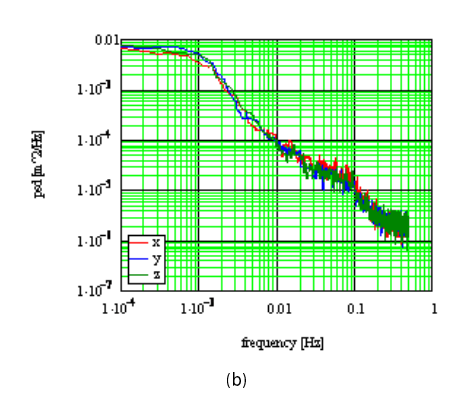


Figure 12. Power spectral densities (Fourier periodograms, mediansmoothed over 31 discrete frequencies) of two residuals with respect to the mean of 5 GPS solutions for aircraft trajectory 141y.



ultimately to the precision in the phase measurement, which depends on the bandwidth of the phase-lock-loop and the signal-to-noise ratio (Jekeli 2000). Hofmann-Wellenhof et al. (1994) give a typical range in the phase noise of between 0.5 mm and 5 mm. Others (e.g., Kyle Snow, Topcon, Inc., personal communication, 2010) quote the precision as approximately 1% of the carrier phase, which for GPS is about 2 mm corresponding to the L1 wavelength of 19 cm, independent of the data rate, provided it is less than the bandwidth of the phase-lock-loop. For the GPS tracking of the aircraft trajectory 141y above, the Allan standard deviation, shown in Figure 13, indicates a noise floor of between 1.5 mm and 3 mm for time intervals of 20 s to 60 s.

The computation of the acceleration along the trajectory 141y using the actual GPS solution thus includes the effect of errors in the positions. In order to isolate this effect from the effect of the model error, we compute the mean of the accelerations for all five solutions and interpret the (negative) residual acceleration with respect to this mean as the error just due to position error. In mathematical terms, if the computed acceleration for the  $i^{th}$  solution is the true acceleration, a, plus acceleration errors due to modeling and positioning errors, respectively,

$$\ddot{x}^{(i)} = a + \varepsilon^{\text{(model)}} + \varepsilon^{\text{(position, }i)}, \tag{27}$$

then the (negative) residual with respect to the mean,  $\ddot{x} = \frac{1}{5} \sum_{i=1}^{5} \ddot{x}^{(i)}$ , is

$$\delta \ddot{x}^{(i)} = \ddot{x}^{(i)} - \ddot{x} = \varepsilon^{(\text{position}, i)} - \frac{1}{5} \sum_{j=1}^{5} \left( \varepsilon^{(\text{position}, j)} \right) \approx \varepsilon^{(\text{position}, i)}.$$
(28)

In this approximation, it is assumed that the model error is the same for each solution (i.e., it does not depend significantly on small variations in the data), and that the average of the position error effects on the computed acceleration per point is negligible compared to the individual effect. Indeed, with the interpretation of the residual as position error, the average residual is identically zero. Consequently, since the differentiation filter is linear, also the *average* acceleration effect per point due to position error is zero. Thus, we conclude that the residual acceleration with respect to the mean of computed accelerations represents the effect of position error, only.

Without applying a moving average along the track, the standard deviations for one set of residual accelerations,  $\delta\ddot{x}_n^{(i)}$ , in the three coordinate directions are approximately:  $\sigma_{\bar{x}}=0.011~\text{m/s}^2$ ,  $\sigma_{\bar{y}}=0.015~\text{m/s}^2$ , and  $\sigma_{\bar{z}}=0.011~\text{m/s}^2$ , respectively. These values were obtained with the central-difference filter and do not change significantly with the order of the filter. Nor do these statistics vary significantly from one set of residuals to the other (different i in equation (28)). We see that the acceleration errors, just due to position error, are greater than the model errors, shown in Figure 6 (for a different trajectory). Figure 14 shows how they change with the degree of smoothing applied to the residuals (i.e., smoothing applied to both the acceleration estimates and the true

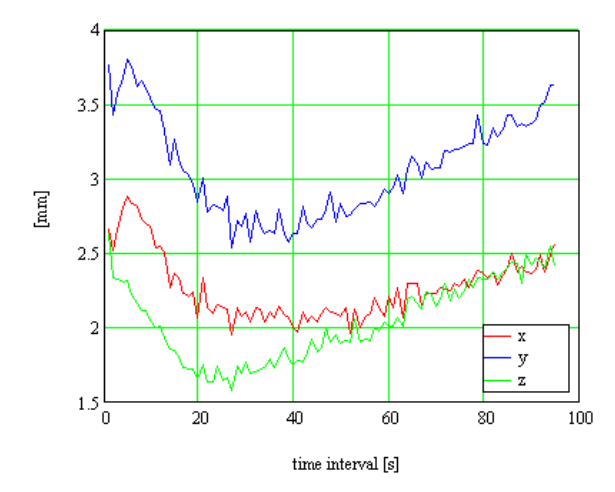


Figure 13. Allan standard deviations of GPS position residuals with respect to the mean of 5 solutions for the 141y flight.

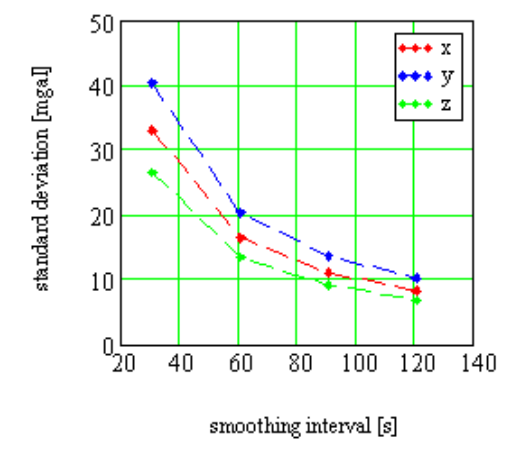


Figure 14. Standard deviations of acceleration residuals relative to the mean of 5 solutions, smoothed along the "141y" trajectory. The central-difference filter with J=60 was used to calculate the accelerations.

acceleration). Only the acceleration standard deviations for one set of residuals are shown, since they are similar for the others.

Also, from the perspective of power spectral densities, the position errors still dominate over the model error. Figure 15 shows the acceleration error psd derived from the psd of the position error (Figure 12) multiplied by the square of the frequency response of the differentiation filter, equation (4). This is compared to the model error psd's obtained when using the J=25 central-difference differentiators. In each of the latter cases (1 Hz and 20 Hz simulated trajectories), the error excludes aliasing effects that would occur if the positions were not first subjected to an efficient anti-aliasing filter.

# Journal of Geodetic Science

0.01 141y position error  $1.10^{-3}$ J=25, 1 Hz simulation  $1.10^{-4}$ 20 Hz simulation 1.10-5 sd [m^2/s^4/Hz] 1.10 1 10<sup>-7</sup> 1.10-8 1 · 10<sup>-9</sup>  $1 \cdot 10^{-10}$  $1 \cdot 10^{-11}$ 1 10<sup>-12</sup> 1.10 0.010.11 10 frequency [Hz]

Figure 15. PSDs of acceleration errors due to position error (red) and model differentiation errors (blue and green).

## 4. Summary

Calculation of the kinematic acceleration is achieved by subjecting the observed positions to a filter whose frequency response approximates the true response associated with a double differentiation in time. Using actual aircraft trajectories derived from GPS, the high-order central-difference filter based on a Taylor expansion of the position function was compared to the second analytical derivative of a B-spline interpolated trajectory. The differences in these second derivatives at points in the trajectory are at the level of several hundred mgal; and, the primary method to yield better performance is subsequent low-pass filtering. Significant smoothing over intervals of 60 s or longer is required to obtain kinematic accelerations with model accuracy at the sub-mgal level. In addition, it was shown that the positions thus used must first be filtered to eliminate aliasing effects due to spectral content beyond the Nyquist frequency associated with the sampling rate. Finally, it was also shown using an aircraft trajectory with known precision that position error from GPS still contributes at least as much to the acceleration error as the model error.

Returning to the question posed at the outset, we find that airborne gravimetry cannot readily take advantage of the phenomenal precision being demonstrated with modern accelerometer technology, which is orders of magnitude superior to the precision of the kinematic acceleration. Both are needed to equal levels of performance. There are two answers to this dilemma (for those pursuing advancements in airborne gravimetry). One is to develop a better tracking system, essentially ranging the aircraft with much higher-frequency carrier waves, e.g., using lasers. The other is to use the accelerometry technology to build new and better gravity gradiometers. Airborne gradiometers are already in use, can measure the very fine structure of the Earth's gravitational field, and do not depend significantly on very precise positioning. Current gradiometry precision is at the level of about 1-2 E (1E = 1 Eötyös =

 $10^{-9} s^{-2}$ ; e.g., Murphy 2010). Therefore, advanced accelerometers with a precision of 10 pg/ $\sqrt{\text{Hz}}$  or better are poised to improve the state-of-the-art in airborne gradiometry.

## Acknowledgments

This investigation was supported by a grant from The Charles Stark Draper Laboratory, Grant No.GRT00021681. Many useful discussions with Tony Radojevic and Shawn Murphy at Draper Lab were very much appreciated. The author is also grateful for the comments of two anonymous reviewers.

## References

Bracewell R, 1965: The Fourier Transform and its Applications. McGraw-Hill Book Company, New York, NY.

Bruton AM, 2000 Improving the accuracy and resolution of SINS/DGPS airborne gravimetry. Report 20145, Dissertation, Department of Geomatics Engineering, University of Calgary, Calgary, Alberta.

Bruton AM, Glennie CL, Schwarz KP, 1999, Differentiation for high-precision GPS velocity and acceleration determination. GPS Solutions, 2(4), 7-21.

Conte SD, de Boor C, 1965: Elementary Numerical Analysis. McGraw-Hill Book Co., New York.

Dickey JO, et al., 1997: Satellite gravity and the geosphere. Report from the Committee on Earth Gravity from Space, National Research Council, National Academy Press.

Draper Laboratory, 2010: Annual Report; Transitioning Technology. http://www.draper.com/annual\_report/AR\_2010.pdf

Forsberg R, Brozena JM, 1992, The Greenland airborne gravity project - comparison of airborne and terrestrial gravity data. Presented at the Seventh Int. Symp.: Geodesy and Physics of the Earth, Potsdam, Germany, October 1992.

Forsberg R, Olesen AV, Keller K, 2001, Airborne gravity survey of the North Greenland continental shelf. In: Sideris M (ed.), Gravity, Geoid, and Geodynamics 2000, IAG Symposia 123, pp.235-240, Springer, Berlin.

Forsberg R, Olesen A, 2009, Geoid determination by airborne gravimetry - principles and applications. Presented at AGU Fall Meeting, 14-18 December 2009, San Francisco, Abstract G65A-01.

Gumert WR, 1998, An historical review of airborne gravimetry. The Leading Edge, 17(1), 113-116.

Hammer S, 1982, Airborne gravity is here! Oil and Gas Journal, January 11, 1982.

Hofmann-Wellenhof B, Lichtenegger H, Collins J, 1994: GPS Theory and Practice. Springer-Verlag, Wien.

Hwang C, Hsiao YS, Shih HC, 2006 Data reduction in scalar air-



## Journal of Geodetic Science

borne gravimetry: Theory, software and case study in Taiwan. Computers & Geosciences, 32, 1573-1584.

Jekeli C, 2000, Inertial Navigation Systems with Geodetic Applications, Walter deGruyter, Berlin.

Jekeli C, Garcia R, 1997, GPS phase accelerations for moving-base vector gravimetry. Journal of Geodesy, 71(10), 630-639. Kennedy SL, Bruton AM, Schwarz KP, 2001, Improving DGPS accelerations for airborne gravimetry: GPS carrier phase accelerations revisited. In: Adam J, Schwarz KP (eds.), Vistas for Geodesy in the New Millennium, IAG Symposia 125, pp.211-216, Springer, Berlin.

Kenyon S , 2000, Arctic Gravity Project - a status. In: Sideris, M. (ed.), Gravity, Geoid, and Geodynamics 2000, IAG Symposia 123, pp.391-395, Springer, Berlin.

Khan IR, Ohba R, 1999: Closed-form expressions for the finite difference approximations of first and higher derivatives based on Taylor series. Journal of Computational and Applied Mathematics, 107, 179-193.

Kreye C, Hein GW, 2003, GNSS based kinematic acceleration determination for airborne vector gravimetry, methods and results. Proceedings of the ION GPS/GNSS 2003 Meeting, Portland, Oregon.

Kwon JH, Jekeli C, 2001: A new approach for airborne vector gravimetry using GPS/INS. J. Geodesy, 74(10), 690-700.

Marple SL, 1987: Digital Spectral Analysis with Applications, Prentice-Hall, Inc., Englewood Cliffs, NJ.

Murphy CA, 2010: Recent developments with Air-FTG. In: R.J.L. Lane (editor), Airborne Gravity 2010 - Abstracts from the ASEG-PESA Airborne Gravity 2010 Workshop: Published jointly by

Geoscience Australia and the Geological Survey of New South Wales, Geoscience Australia Record 2010/23 and GSNSW File GS2010/0457.

NASA, 1991, Solid Earth Science in the 1990's, The Coolfont Report, NASA Tech. Mem. 4256, vol.1-3, NASA Office of Space Science and Applications.

National Research Council, 1995, Airborne geophysics and precise positioning: scientific issues and future directions. Report of the Committee on Geodesy, T. Herring (chair), National Research Council, National Academic Press, Washington, D.C.

Parks TW, McClellan JH, 1972: Cheyshev approximation for nonrecursive digital filters with linear phase. IEEE Trans. Circuit Theory, 19(2), 189-194.

Salazar D, Hernandez-Pajares M, Juan-Zornoza JM, Sanz-Subirana J, Angela Aragon-Angel A, 2011: EVA: Extended velocity and acceleration determination. Journal of Geodesy, in press.

Schumaker LL, 1993: Spline functions: Basic Theory. Wiley, New York.

Shan S, Bevis M, Kendrick E, Mader GL, Raleigh D, Hudnut K, Sartori M, Phillips D, 2007: Kinematic GPS solutions for aircraft trajectories: identifying and minimizing systematic height errors associated with atmospheric propagation delays. Geophysical Research Letters, 34, L23S07, doi: 10.1029/2007/GL030889. Van Dierendonck KJ, Cannon ME, Wei M, Schwarz KP, 1994: Error sources in GPS-determined acceleration for airborne gravimetry. Proceedings of the ION National Technical Meeting, San

Diego, CA, 24-26 January 1994, pp.811-820.

